Supporting Information

Construction of Sn-P-Graphene microstructure with Sn-C and P-C co-bonding as anodes for Lithium-ion battery

Yuanxing Zhang, Li Sun*, Xiaoxue Zhao, Lin Wu, Ke Wang, Haochen Si, Jialin Gu, Chao Sun, Yan Shi and Yihe Zhang

Beijing Key Laboratory of Materials Utilization of Nonmetallic Minerals and Solid Wastes, National Laboratory of Mineral Materials, School of Materials Science and Technology, China University of Geosciences, Beijing, No. 29, Xueyuan road, Haidian district, Beijing 100083, PR China

**Corresponding author: sunli@cugb.edu.cn*

Experimental Section

Synthesis of Sn_4P_3 and Sn_4P_3@G : Sn_4P_3@G composite was prepared by two-step High Energy ball milling (HEBM). In the first step, $Sn_4P_3$was prepared with 4:3 amount of substance of tin (ALADDIN T108793-50g, 99.5%) and amorphous Red Phosphorus (alfa 010281, > 98.9%). The ball milling process was carried out in Ar atmosphere at 375 rpm for 20 hours, and the ball powder ratio was 20:1. In the second step, the Sn_4P_3 powder was milled with 30 wt% Expanded Graphite (3000 mesh) under an Ar atmosphere at 375 rpm with a ball to powder ratio of 25 : 1.

Synthesis of P-Sn@G composites and different proportions : All the P-Sn@G composites was prepared by one-step High Energy ball milling. The ratio of amount of substance of tin and Red Phosphorus in all reactant is 4:3. The tin and amorphous red phosphorus were milled with Expanded Graphite (3000 mesh) under an Ar atmosphere at 375 rpm with a ball to powder ratio of 25: 1. The mass content ratio of graphene is 10 wt%, 20 wt%, 30 wt%, 40 wt%, 50 wt%. The product numbers obtained are P-Sn@G91, P-Sn@G82, P-Sn@G73, P-Sn@G64, P-Sn@G55. To ensure that the reaction process of ball milling is free from air interference, weighing of reactants and the ball milling tank are sealed in the glove box(O_2<0.1ppm) filled

with Ar.

Synthesis of FLG : The FLG was prepared by one-step High Energy ball milling. The Expanded Graphite (3000 mesh) under an Ar atmosphere at 375 rpm with a ball to powder ratio of 25: 1.

Material Characterizations: The scanning electron microscope (SEM) images were obtained by Zeiss SIGMA 500. Transmission electron microscopy (TEM) images and high-resolution transmission electron microscopy (HRTEM) images were obtained by JEM-2010 F. X-ray powder diffraction (XRD) (Bruker Scientific Instruments Hong Kong CO., Limited, D8 Advance) were characterized Cu Kα radiation (λ= 1.5418 Å) in the 2θ degrees ranged from 20° to 90°. BX-ray photoelectron spectroscopy (XPS) measurements were characterized by a Kratos-Axis spectrometer with monochromatic Al Kα (1,486.71 eV) X-ray radiation (15 kV and 10 mA).

Electrochemical measurements for LIBs: The Lithium storage behavior was evaluated using CR2016-type coin cells, with the prepared materials as the working electrode, lithium foil as the counter/reference electrode($LiNi_{0.5}Mn_{1.5}O_4$ as cathode), Celgard 2400 microporous film as the separator, and 1 M $LiPF_6$ in a 1:1 (v/v) EC/DEC as electrolyte. Extra additives (5% FEC) used in the electrolyte in the Full-cell. Coin-type half/full-cells were assembled in a glove box filled with protective argon gas (M. Braun inert gas systems Co. Ltd., Germany). The working electrodes were prepared using a slurry casting method. The active materials, super-P and PVDF were mixed with weight ratio of 8:1:1 to form homogenous slurry with NMP, then casted onto copper foil (Cathode onto aluminum foil) with a doctor blade. The diameter of the copper foil is 1 cm, and the loading mass of the active materials on each electrode was about 0.6-1.1 $mg \cdot cm^{-2}$. The mass ratio of active materials in the negative/positive electrodes is about 1.2. The GCD tests were conducted on a Land battery test system (Wuhan Land Electronic Co., China) in a voltage (vs. Li^+ /Li) window of 0.01-3 V (0-4.9 V for full-cell). CV tests were performed at a scanning rate of 0.2 to 5 $mV \cdot s^{-1}$. EIS spectra were collected in the frequency range from 100 kHz to 10 mHz.

Calculations: Calculation method for capacitance contribution：

According to the following formula : $i\,(V) = k_1\,v^{1/2} + k_2 v$, For the convenience of calculation $i\,(V)/\,v^{1/2} = k_1\, + k_2 v^{1/2}$ where $k_2 v$ represents the contribution of capacitance behaviour, and k_1 and k_2 could be obtained by slope and intercept of $v^{1/2}\ to\ i\,(V)/\,v^{1/2}$, the capacitance and diffusion contribution of specific voltage can be calculated.

The contribution of capacitance can be qualitatively analyzed by the following formula: $i(V) = av^b$ where both a and b are adjustable parameters. The value of *b* is calculated by the slope of log(*i*) and log(*v*). The *b* value of 1 indicates a capacitive process, and the *b* value of 0.5 reveals a diffusion-controlled process.

Calculation method of diffusion coefficient:

$$D = (4/\pi\Delta t)(m_B V_M/M_B S)(\Delta E_S/\Delta E_\tau)^2$$

Where Δt is the constant current pulse time, m_B is the mass of the electrode, M_B and V_M are the molar mass and molar volume of the electrode, S is the total contact area between the electrolyte and the electrode; ΔE_s and ΔE_τ can be obtained from Fig. 3b, which represent the changes in steady-state voltage after excluding the IR drop and the all transient change in half-cell voltage during a single titration.

Figure S18 shows the electrode thickness is about 10 μm. Unified unit for calculation

Calculation method of energy density *(E)* and power density*(P)* of full-cell:

$$Electrode\ density(g{\cdot}ml^{-1}) = \frac{Mass\ loading\ (g{\cdot}cm^{-2})}{Electrode\ thickness\ (cm)}$$

$$Volumetric\ capacity(Ah{\cdot}l^{-1}) = Eravimetric\ capacity\ (mAh{\cdot}g^{-1}) \times\ Electrode\ density(mAh{\cdot}ml^{-1})$$

$$Energy\ density(Wh{\cdot}l^{-1}) = Volumetric\ capacity(Ah{\cdot}l^{-1}) \times\ Voltage(V)$$

$$Power\ density(W{\cdot}l^{-1}) = Current\ density(A{\cdot}l^{-1}) \times Voltage(V)$$

Supplementary Figures

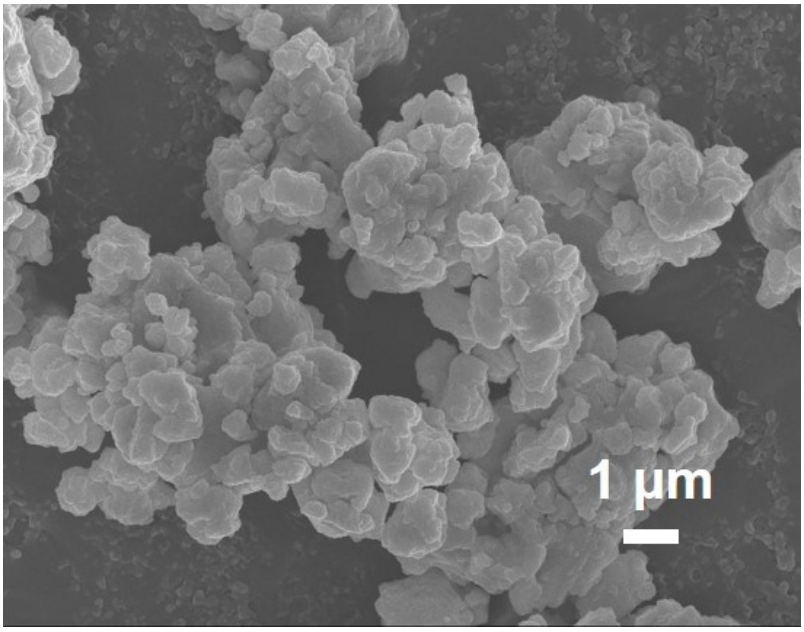

Figure S1 SEM image Sn_4P_3

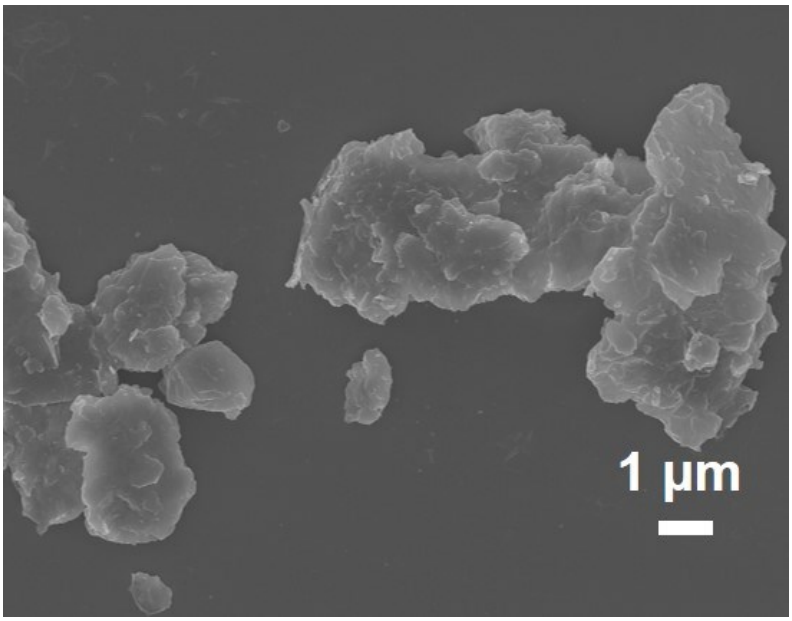

Figure S2 SEM image Sn_4P_3@G

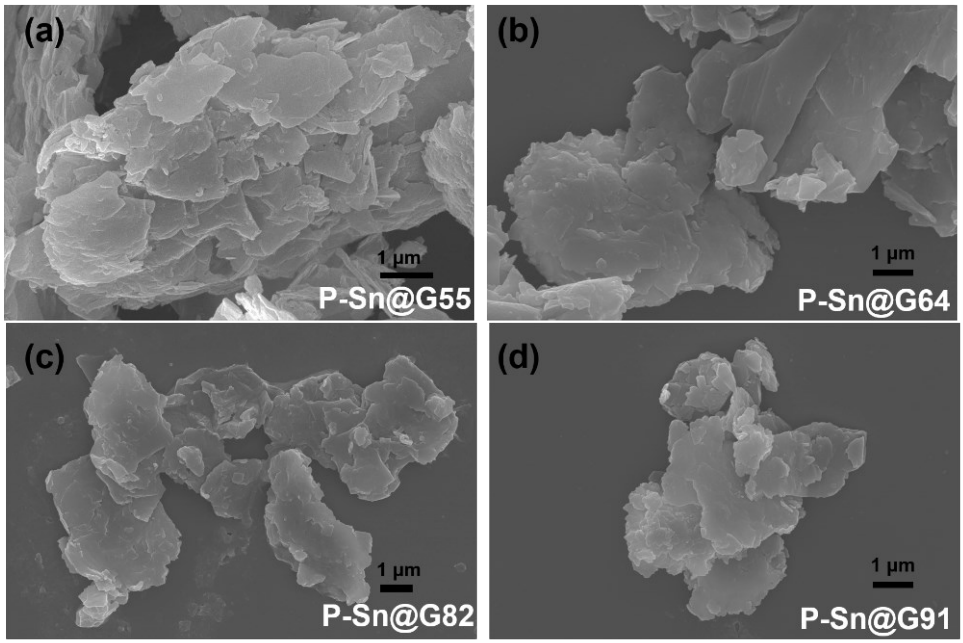

Figure S3 SEM images of (a) P-Sn@G55 (b) P-Sn@G64 (c) P-Sn@G82 (d) P-Sn@G91.

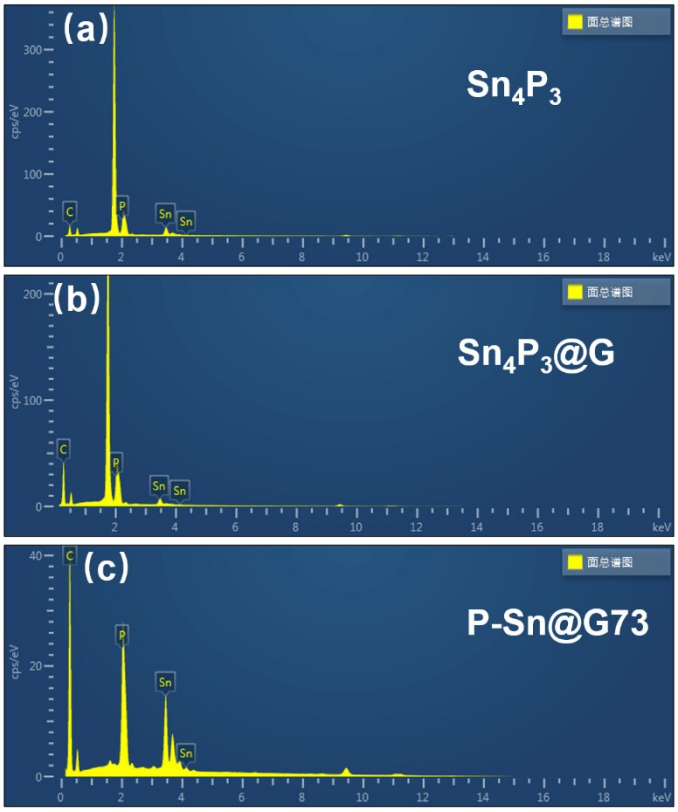

Figure S4 SEM EDX result of (a) Sn_4P_3, (b) Sn_4P_3@G and (c) P-Sn@G73.

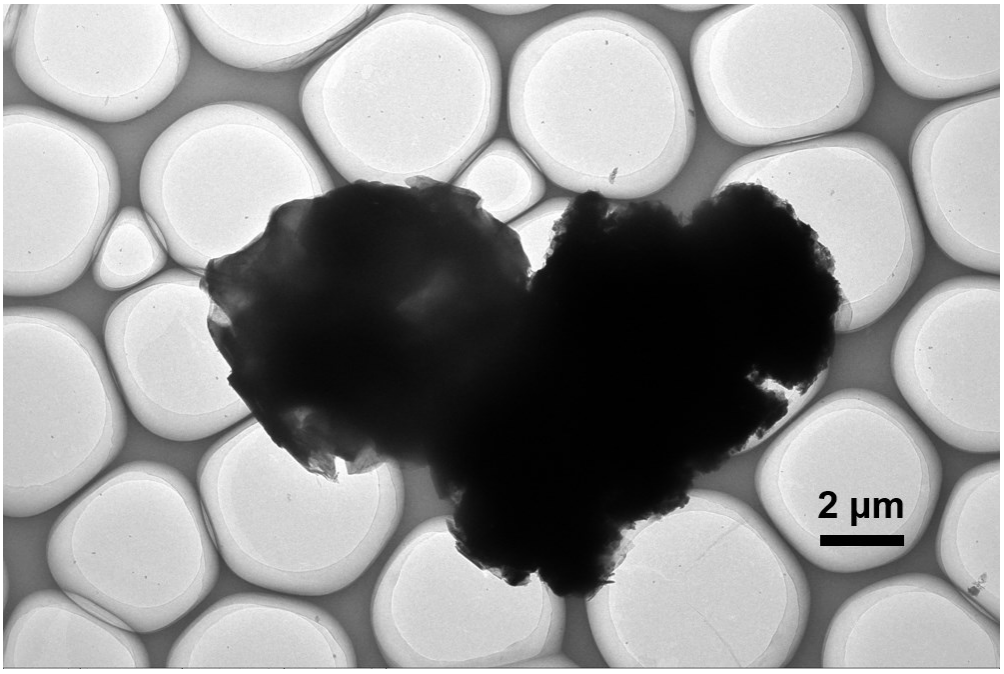

Figure S5 Low magnification TEM image P-Sn@G73

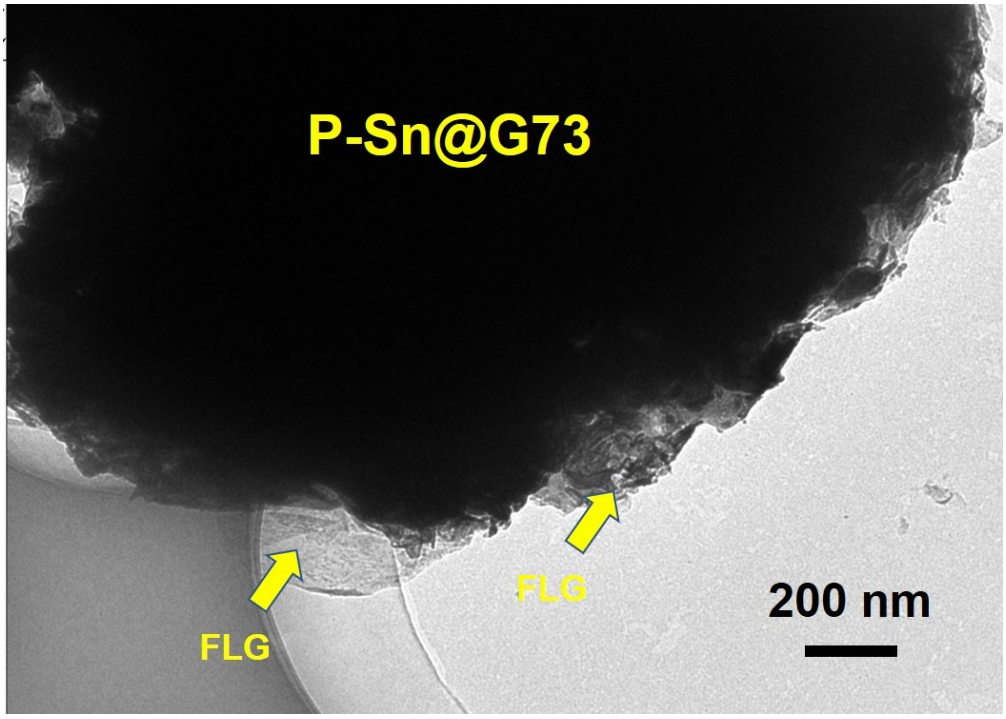

Figure S6 High magnification TEM image P-Sn@G73

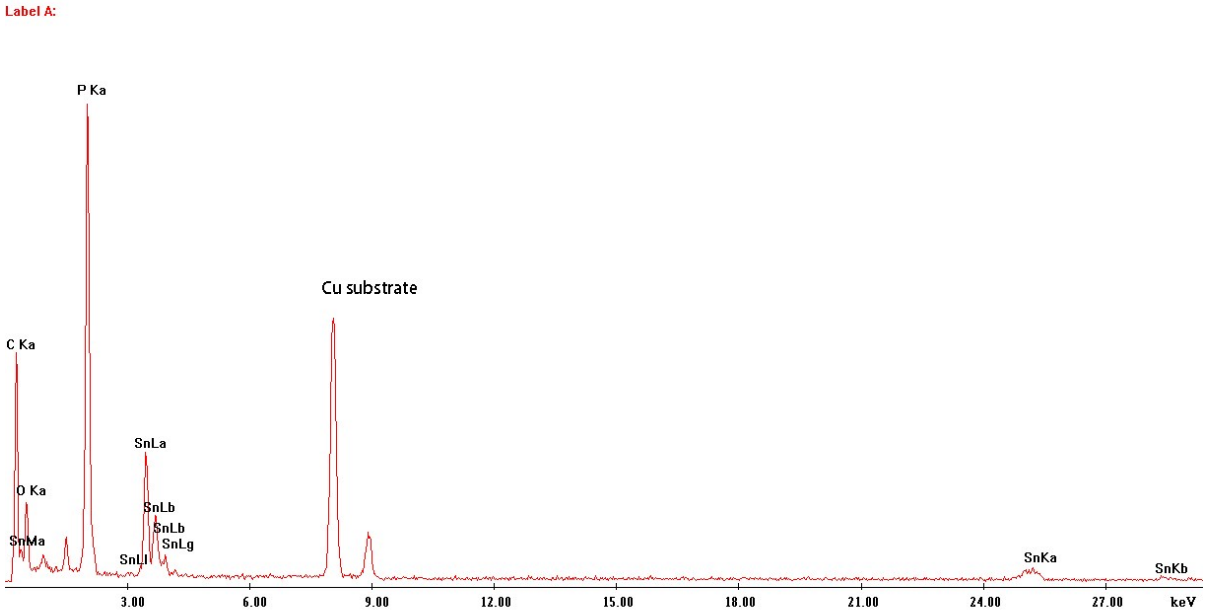

Figure S7 TEM EDX result of P-Sn@G73

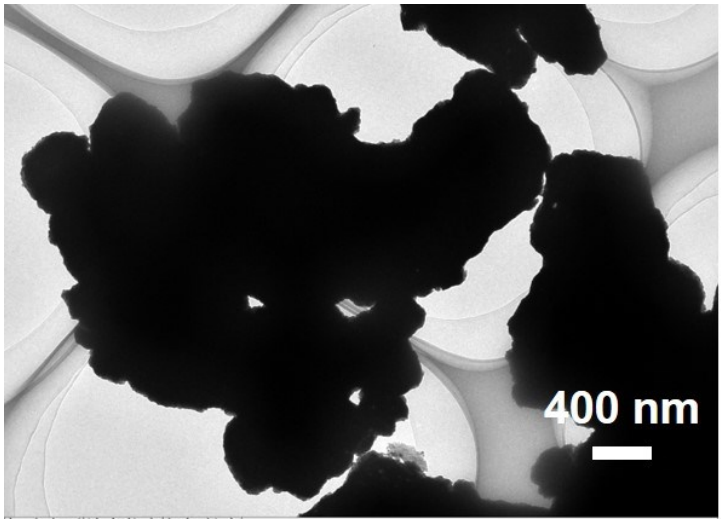

Figure S8 TEM image Sn_4P_3

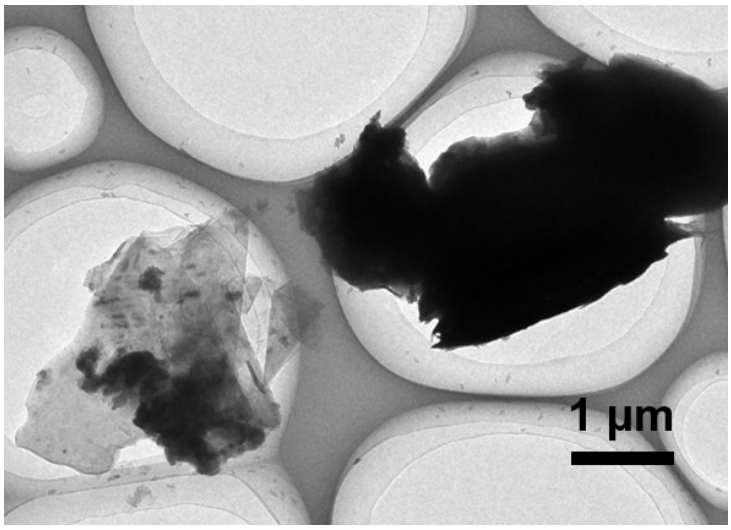

Figure S9 TEM image Sn_4P_3@G

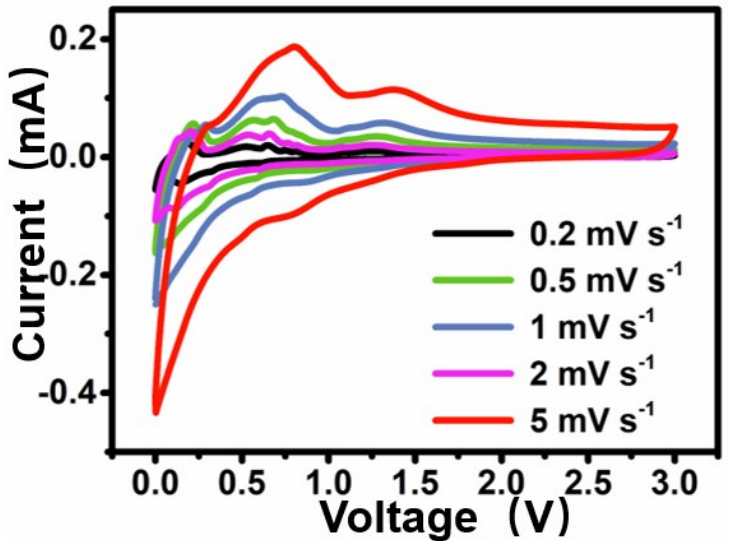

Figure S10 (a) CV curves of P-Sn@G73 electrode

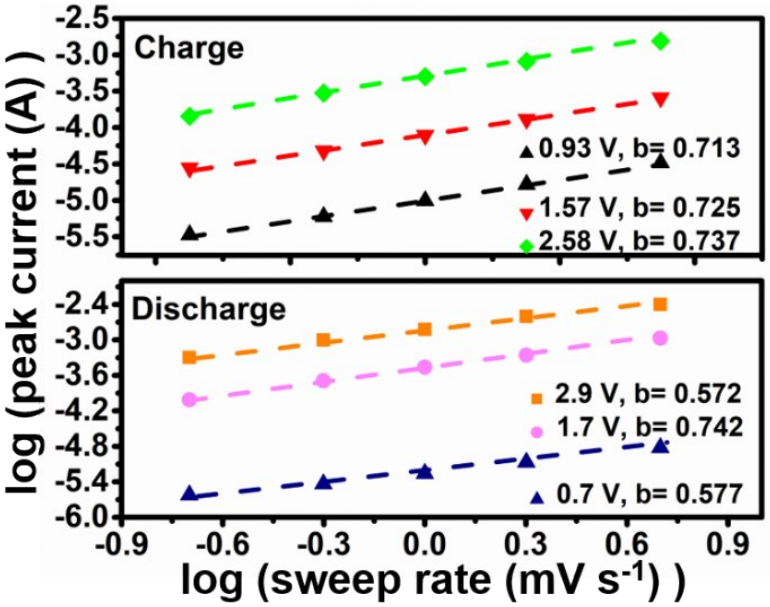

Figure S11 Determination of *b*-values at different potentials.

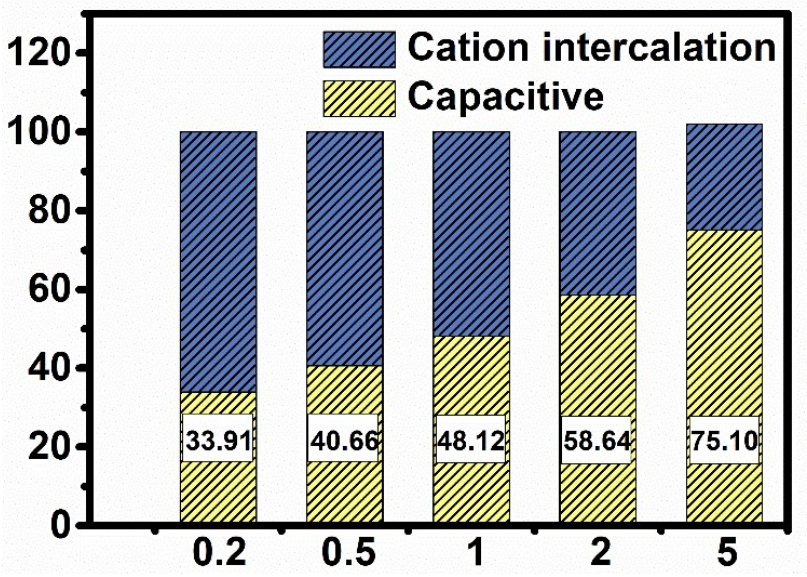

Figure S12 Contribution ratio of the capacitive and cation intercalation-controlled currents.

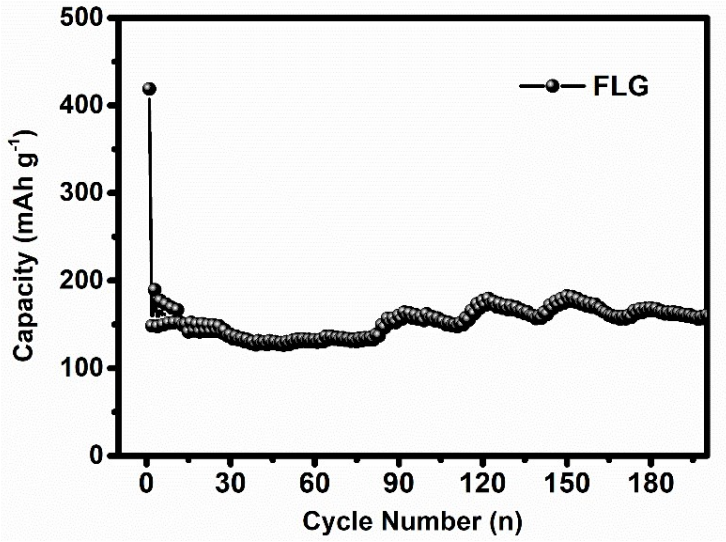

Figure S13 Cycle performance at 0.2 $A \cdot g^{-1}$ for FLG

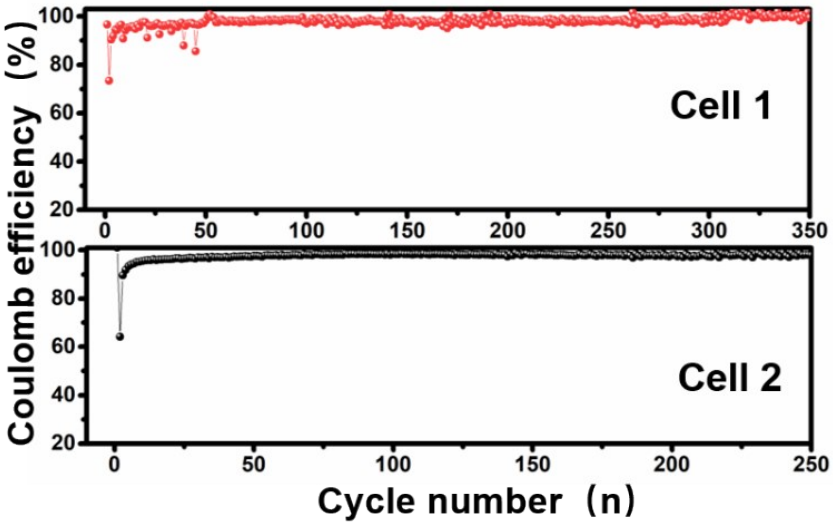

Figure S14 Coulomb efficiency of two half-cell. (Cell 1 for rate test, Cell 2 for cycle test.)

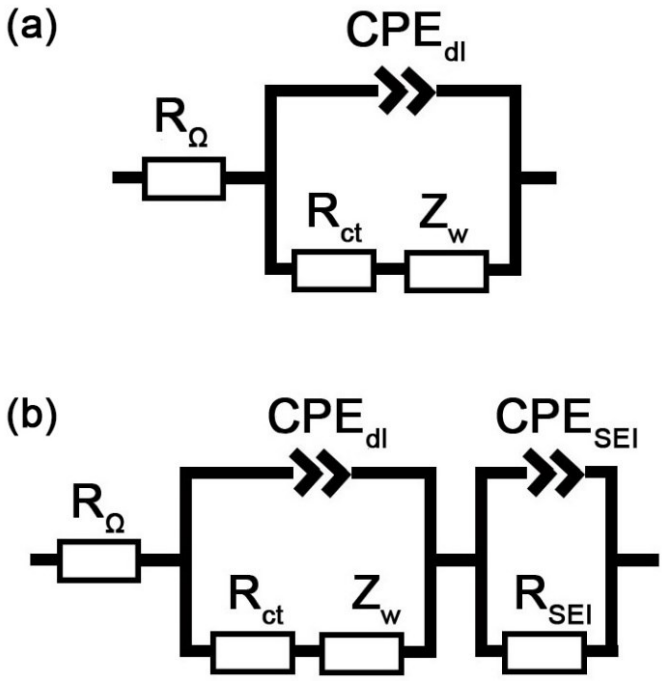

Figure S15 (a) Equivalent circuit model for the electrodes before and (b) after 10 cycles

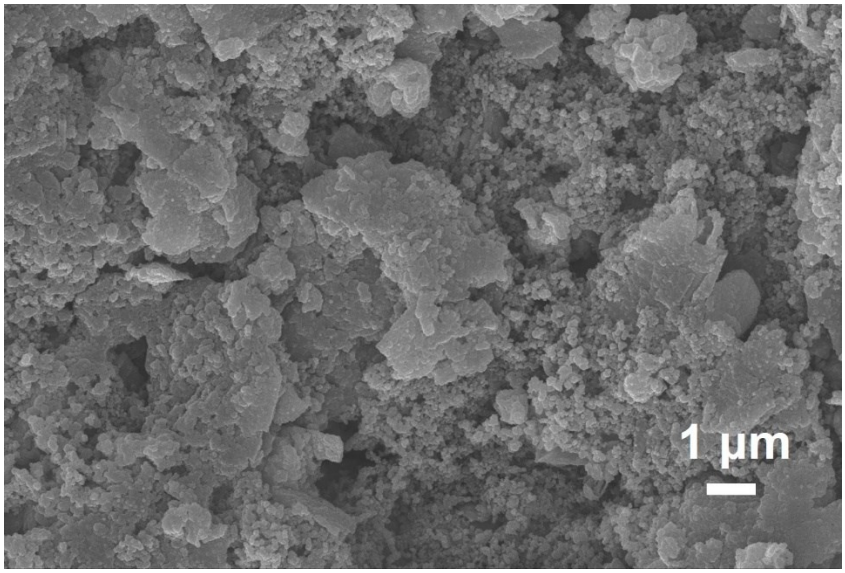

Figure S16 After cycling and SEM image of after P-Sn@G73 electrode.

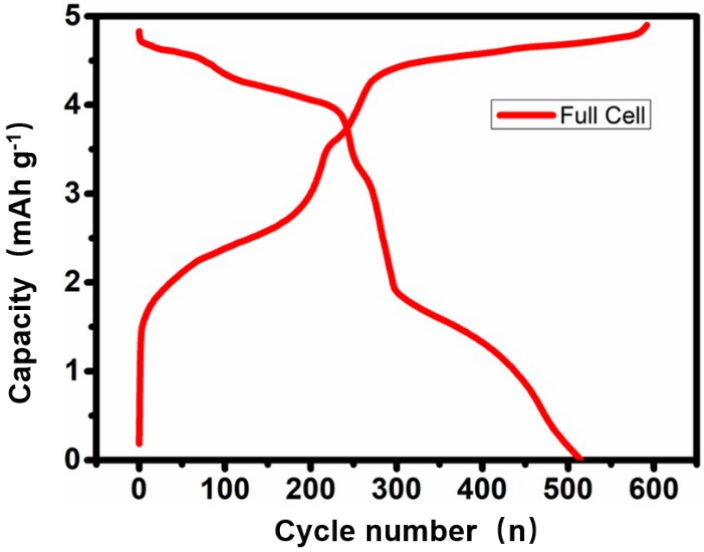

Figure S17 Charge discharge curve of the of full-cell

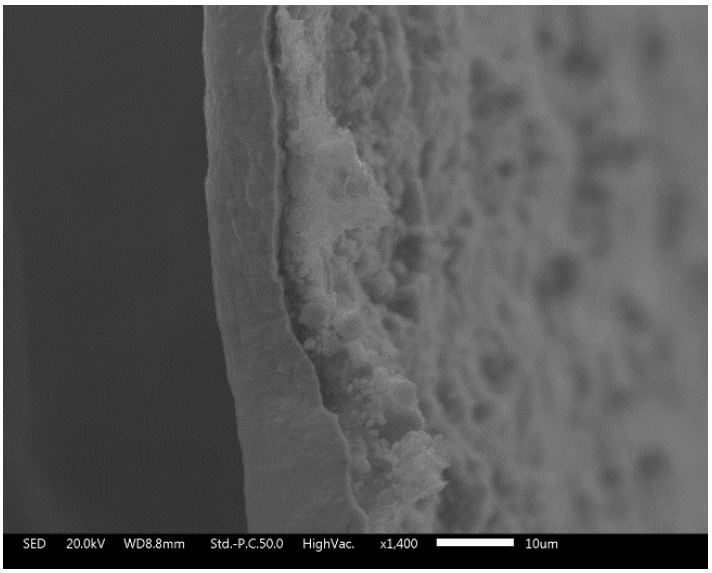

Figure S18 Electrode thickness is about 10 μm.

Table S1 EIS parameters of LIBs for the P-Sn@G73

Samples	Resistance (Ω)			CPE_{dl}		CPE_{SEI}	
	R_Ω	R_{SEI}	R_{ct}	(S s^n)	n_1	(S s^n)	n_2
P-Sn@G73	3.52	-	63.3	9.142×10^{-5}	0.71	-	-
after 10 cycles	3.48	8.75	31.1	3.155×10^{-3}	0.57	3.64×10^{-6}	0.74

R_Ω corresponds to the Ohmic resistance from current collectors, separator, electrode, and electrolyte, The radius of the semicircle can be interpreted as the transfer resistance (R_{ct}) between the charge electrode and the electrolyte, CPE_{dl} relates to the non-ideal capacitance of double layer capacitance, R_{SEI} and CPE_{SEI} correspond to resistance and non-ideal capacitance of the SEI layer introduced after cycling.

Table S2 A survey of alloying type Sn-P based anode materials for LIBs.

Anode Materials	Reversible Capacity	Rate Capability	Refs
P-Sn@G73	1068.5 mAh g^{-1} @200 mA g^{-1}	360.8 mAh g^{-1} @8000 mA g^{-1}	This work
Sn_4P_3/GS	606.4 mAh g^{-1}@100 mA g^{-1}	254.4 mAh g^{-1} @100 mA g^{-1}	1
Fe-Sn-P alloys	427 mAh g^{-1}@100 mA g^{-1}	-	2
Sn_xP_y@C	718 mAh g^{-1}@100 mA g^{-1}	370 mAh g^{-1} @1000 mA g^{-1}	3
Sn_4P_3 nanoparticles	442 mAh g^{-1} @100 mA g^{-1}	210 mAh g^{-1} @500 mA g^{-1}	4
Sn_4P_3/SnO_2@C	733 mAh g^{-1} @200 mA g^{-1}	713 mAh g^{-1}@2000 mA g^{-1}	5
Sn_4P_3-C	1255 mAh g^{-1} @200 mA g^{-1}	380 mAh g^{-1}@4000 mA g^{-1}	6
Ni-Sn-P@C-CNT	704 mAh g^{-1} @100 mA g^{-1}	293 mAh g^{-1}@500 mA g^{-1}	7
Sn/graphene	390 mAh g^{-1} after 50 cycles	-	8
Sn/G/GNS	557 mAh g^{-1} after 200 cycles	-	9

Table S3 Ragone plot table for Fig 4f

Anode Materials	Wolumetric energy density (Wh L^{-1})	Power density(W l^{-1})	Refs
P-Sn@G73	1122.9	21019	This work
N-PSi@C//LFP	1621	~1200	10
N-PSi@C//LCO	~750	7762	10
ATO-LCO/ATO-Si	1625	3300	11
graphite/SEAG	1060	2800	12
Nb16W5O55/LMO	300	980	13
Nb18W16O93/LMO	400	1080	13
T-Nb2O5/LMO	60	1060	13

References

1 Y. Jiang, Y. Wang, J. Jiang, S. Liu, W. Li, S. Huang, Z. Chen and B. Zhao, *Electrochim. Acta*, 2019, **312**, 263–271.

2 X. M. Zheng, P. Y. Zhang, L. K. Wang, S. Tao, Y. X. Wang, L. Huang, J. T. Li and S. G. Sun, *Electrochim. Acta*, 2017, **247**, 314–320.

3 M. Zhang, H. Wang, J. Feng, Y. Chai, X. Luo, R. Yuan and X. Yang, *Appl. Surf. Sci.*, 2019, **484**, 899–905.

4 S. Liu, H. Zhang, L. Xu, L. Ma and X. Chen, *J. Power Sources*, 2016, **304**, 346–353.

5 Y. Xia, S. Han, Y. Zhu, Y. Liang and M. Gu, *Energy Storage Mater.*, 2019, **18**, 125–132.

6 J. Choi, W. S. Kim, K. H. Kim and S. H. Hong, *J. Mater. Chem. A*, 2018, **6**, 17437–17443.

7 R. Dai, W. Sun, L. P. Lv, M. Wu, H. Liu, G. Wang and Y. Wang, *Small*, 2017, **13**, 1–11.

8 J. Zhu, A. Liu and D. Wang, *Appl. Surf. Sci.*, 2017, **416**, 751–756.

9 J. Zhu and X. Ding, *J. Alloys Compd.*, 2019, **809**, 151870.

10 B. Wang, J. Ryu, S. Choi, X. Zhang, D. Pribat, X. Li, L. Zhi, S. Park and R. S. Ruoff, *ACS Nano*, 2019, **13**, 2307–2315.

11 J. I. Lee, E. H. Lee, J. H. Park, S. Park and S. Y. Lee, *Adv. Energy Mater.*, 2014, **4**, 1–9.

12 N. Kim, S. Chae, J. Ma, M. Ko and J. Cho, *Nat. Commun.*, 2017, **8**, 1–10.

13 A. S. Lakhnot, T. Gupta, Y. Singh, P. Hundekar, R. Jain, F. Han and N. Koratkar, *Energy Storage Mater.*, 2020, **27**, 506–513.